

FULL PAPER

Open Access

# Volatile (F and Cl) concentrations in Iwate olivine-hosted melt inclusions indicating low-temperature subduction

Estelle F Rose-Koga<sup>1\*</sup>, Kenneth T Koga<sup>1</sup>, Morihisa Hamada<sup>2</sup>, Thomas Hélouis<sup>1</sup>, Martin J Whitehouse<sup>3</sup> and Nobumichi Shimizu<sup>4</sup>

## Abstract

Investigation of olivine-hosted melt inclusions provides information about the abundance of volatile elements that are often lost during subaerial eruptions of lavas. We have measured the abundances of H<sub>2</sub>O, CO<sub>2</sub>, F, Cl, and S as well as Pb isotopes in 29 melt inclusions in the scoria of the 1686 eruption of the Iwate volcano, a frontal-arc volcano in the northeast Japan arc. Pb Isotope compositions identify that Iwate magma is derived from a mixture of depleted mantle, subducted basalt, and sediment. Systematics of F in comparison to MORB and other arc magma indicates that (1) the slab surface temperature must be among the lowest on Earth and (2) hydrous minerals, such as amphibole, humites, and/or mica, must be present as residual phases during the dehydration of the slab.

## Introduction

Japan arc lavas display a wide range of compositions mainly interpreted as involving aqueous fluids released from the subducting plates (e.g., Nakamura and Iwamori 2009 and references therein). Iwate volcano, is situated in the northeastern (NE) Japan arc (Figure 1), and mainly consists of Quaternary low-K basalts and andesites (e.g., Itoh and Doi 2005; Kuritani et al. 2013). The chemical variations of the Iwate lavas have been attributed to the different proportion of fluids coming from sediment and/or altered oceanic crust (Shibata and Nakamura 1997; Sano et al. 2001; Hanyu et al. 2006). Both velocity tomography measurements in the mantle wedge above the slab and mapping of earthquake size distribution within the slab point towards a fluid source located right above of the slab at depths of 140 to 150 km (Wyss et al., 2001). The pre-eruptive volatile content of these magmas is of fundamental importance to understand the chemistry of the fluids after their interaction with the mantle wedge. Fluid chemistry will elucidate melting processes and characterize the source mantle. Since major volatile elements (H<sub>2</sub>O, CO<sub>2</sub>,

SO<sub>2</sub>) will have degassed from the erupted lava, melt inclusions trapped in early crystallizing olivine carry the best chance of retaining dissolved volatiles of magmas at depth (e.g., Sobolev 1996).

However, a note of caution is sounded because melt inclusions are leaky containers for H<sub>2</sub>O (Chen et al. 2011; Gaetani et al. 2012). CO<sub>2</sub> solubility in silicate melt is significantly lower than that of H<sub>2</sub>O and therefore CO<sub>2</sub> degassing begins earlier during magma ascent, i.e. from a deeper depth (e.g. Shishkina et al. 2010). Therefore, the CO<sub>2</sub> concentration measurements in melt inclusions is at best considered as minimum values. Sulfur concentrations measured in melt inclusions also display a degassing trend (e.g. Spillaert et al. 2006). In the present olivine-hosted melt inclusion study we use F and Cl concentrations to assess the pre-degassed volatile compositions of the basaltic melt underneath Iwate volcano, Japan. We report that the volatile contents of Iwate magma are (i) solely due to fluids coming from the slab and (ii) the source region of the mantle wedge undergoing partial melting is highly depleted.

## Samples and methods

The Iwate samples are some of the least differentiated rocks on the volcanic front of the Japanese island arcs (Figure 1). The olivine-hosted melt inclusions of the scoria

\* Correspondence: e.koga@opgc.univ-bpclermont.fr

<sup>1</sup>Laboratoire Magmas et Volcans, Université Blaise Pascal, CNRS, UMR 6524, IRD, R 163, Clermont-Ferrand 63038, France

Full list of author information is available at the end of the article

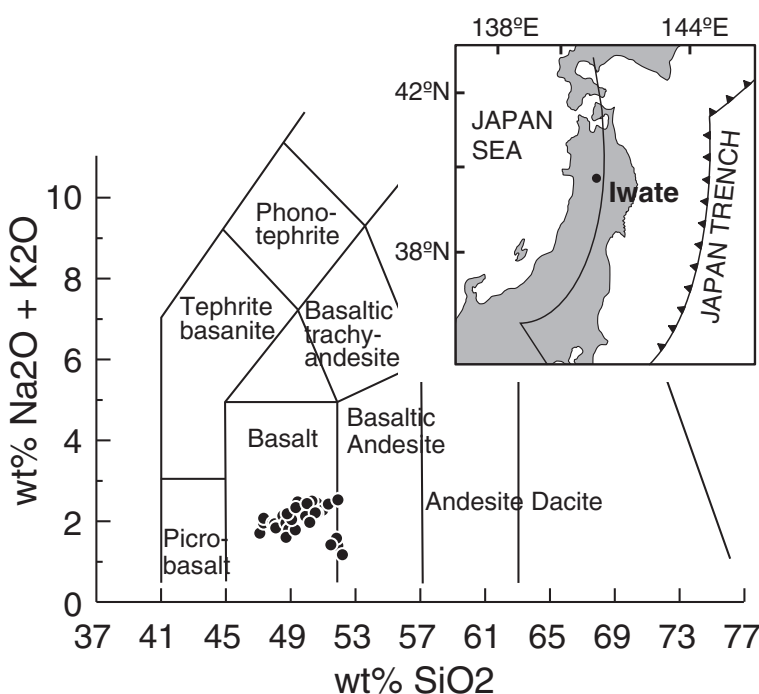


**Figure 1** Diagram reporting  $\text{SiO}_2$  as a function of  $\text{K}_2\text{O}$  and  $\text{Na}_2\text{O}$  (wt.%) of the Iwate glassy melt inclusions. The all fall in the basalt domain with few of them touching the basaltic-andesite domain. Inset: map of NE Japan arc. The volcanic front is indicated by a line. Iwate volcano is a front arc volcano.

of the 1686 eruption of Iwate volcano are basaltic to basaltic-andesitic in composition (Figure 1). Olivine crystals are separated from the rock and 34 glassy melt inclusions were selected for major elements among which 29 were also analyzed for volatiles and Pb-isotopes. The hand sample is olivine, plagioclase, and rare pyroxene-phyric. The olivine phenocrysts range from <0.5 to 2 mm in size. Primary melt inclusions are easily found in the olivines, but only the glassy (much scarcer) inclusions were selected. No secondary melt inclusions were observed in the olivines, but some were observed in the pyroxenes.

Volatile concentrations ( $\text{H}_2\text{O}$ ,  $\text{CO}_2$ ,  $\text{F}$ ,  $\text{S}$ , and  $\text{Cl}$ , Table 1) were measured by SIMS at WHOI (Woods Hole, MA, USA) and EMP at LMV (Clermont-Ferrand, France). The mono-collection SIMS settings are detailed in other studies (Rose-Koga et al. 2008; additional file 2: table S5 in Hélo et al. 2011; Rose-Koga et al. 2012) and summarized in the following: we used a  $\text{Cs}^+$  primary beam with a current of 1.5 nA. The electron gun was used to avoid charging of the sample surface. The sample was pre-sputtered for 3 min with a  $30 \times 30 \mu\text{m}$  square raster, and analyses were performed on the central  $15 \times 15 \mu\text{m}$  area, centered in the rastered area by a mechanical aperture placed at the secondary ion image plane. The instrument was operated with a mass resolving power of 6,600, allowing complete discrimination of interferences ( $^{34}\text{S}^1\text{H}$  on  $^{35}\text{Cl}$ ,  $^{17}\text{O}$  on  $^{16}\text{O}^1\text{H}$ ,  $^{29}\text{Si}^1\text{H}$  on  $^{30}\text{Si}$ , and  $^{31}\text{P}^1\text{H}$  on  $^{32}\text{S}$ .

We used a critical illumination method. A  $400 \mu\text{m}$  contrast aperture was used and the energy slit opening was  $\pm 30 \text{ eV}$ . Including pre-sputter time, each measurement lasted approximately 15 min. The maximum uncertainties, taking into account the reproducibility over 10 cycles of analyses and the uncertainties on the regression of the calibration line, were less than 5% for  $\text{H}_2\text{O}$ , 15% for  $\text{CO}_2$ , and 10% for  $\text{Cl}$ ,  $\text{F}$ , and  $\text{S}$ .

Cerium concentration measurements were performed with the WHOI 1280 SIMS. The duoplasmatron with a  $10 \text{nA } ^{16}\text{O}^-$  primary beam was used. A 10 kV secondary voltage was placed on the sample to accelerate the secondary ions and an energy filtering of  $-90 \text{ V}$  was applied (e.g., Shimizu and Hart, 1982). A  $20 \mu\text{m}$  contrast aperture is used, and a mass resolution power of 1,250 is achieved by setting the entrance slit at 405 mm and exit slit at 972 mm. A deadtime correction of 28 ns is applied. Prior to the analysis, a pre-sputter of 240 s was performed and the total analysis time is  $\sim 20$  min. During each analysis cycle, intensities for the following isotopes were collected:  $^{30}\text{Si}$  (5 s),  $^{88}\text{Sr}$  (10 s),  $^{89}\text{Sr}$  (10 s),  $^{90}\text{Zr}$  (10 s),  $^{93}\text{Nb}$  (10 s),  $^{138}\text{Ba}$  (10 s),  $^{139}\text{La}$  (10 s), and  $^{140}\text{Ce}$  (10 s). The beam size (nA) and duration of each measurement were adjusted (decreased and increased, respectively) to accommodate the measurement of small-diameter melt inclusions. We used the basaltic reference glasses KL2-G and ALV519-4-1, to generate the working curves and

**Table 1 major element concentrations (in wt%), corrected from olivine addition, of 34 glassy olivine-hosted melt inclusions from Iwate volcano**

Olivine addition (%)	SiO <sub>2</sub>	MgO	FeO	MnO	K <sub>2</sub> O	CaO	Na <sub>2</sub> O	Al <sub>2</sub> O <sub>3</sub>	TiO <sub>2</sub>	P <sub>2</sub> O <sub>5</sub>	
ITM1.1	4.8	48.9(4)	7.89(10)	11.2(3)	0.15(7)	0.070(1)	8.45(6)	1.75(7)	16.2(2)	0.71(1)	0.040(2)
ITM1.2	3.2	48.9(4)	7.37(9)	10.5(3)	0.2(1)	0.100(2)	8.33(6)	1.87(7)	16.1(2)	0.84(1)	0.120(7)
ITM2	7.0	48.9(4)	7.59(10)	12.9(4)	0.19(9)	0.090(2)	8.14(6)	2.08(8)	14.5(2)	0.87(1)	0.080(5)
ITM5.1	6.0	48.6(4)	7.51(10)	11.1(3)	0.16(7)	0.090(2)	9.07(7)	2.02(8)	16.8(2)	0.72(1)	n.d.
ITM5.2	10.2	50.7(5)	8.14(10)	12.1(4)	0.18(8)	0.110(2)	8.90(7)	2.33(9)	15.3(2)	0.85(1)	0.030(2)
ITM6	6.8	48.8(4)	8.02(10)	12.0(4)	0.18(9)	0.140(3)	9.12(7)	1.71(7)	16.2(2)	0.76(1)	n.d.
ITM8	10.4	48.2(4)	9.26(12)	12.2(4)	0.11(5)	0.150(3)	8.87(7)	1.67(7)	15.3(2)	0.80(1)	0.070(4)
ITM10.1	10.6	50.6(5)	7.55(10)	10.4(3)	0.2(1)	0.150(3)	8.81(7)	2.03(8)	15.2(2)	0.81(1)	0.040(2)
ITM10.2	13.6	50.3(5)	7.32(9)	10.1(3)	0.18(8)	0.070(2)	8.65(7)	1.88(8)	16.8(2)	0.65(1)	0.050(3)
ITM11	6.8	51.0(5)	7.56(10)	10.9(3)	0.17(8)	0.170(4)	8.15(6)	2.08(8)	15.2(2)	0.73(1)	0.150(9)
ITM12	4.8	48.3(4)	7.97(10)	11.0(3)	0.2(1)	0.100(2)	8.97(7)	1.78(7)	16.1(2)	0.70(1)	0.150(9)
ITM13	8.0	48.0(4)	8.31(11)	10.9(3)	0.14(6)	0.110(2)	9.34(7)	1.83(7)	16.4(2)	0.70(1)	0.080(5)
ITM14	9.4	52.0(5)	8.25(11)	11.4(3)	0.17(8)	0.220(5)	8.71(7)	1.32(5)	15.2(2)	0.86(1)	0.150(9)
ITM15.1	8.0	50.5(5)	6.91(9)	12.0(4)	0.17(8)	0.190(4)	8.18(6)	2.29(9)	14.9(2)	1.01(1)	0.040(2)
ITM15.2	7.8	51.5(5)	7.02(9)	12.2(4)	0.3(1)	0.140(3)	8.20(6)	2.25(9)	14.4(2)	0.97(1)	0.140(8)
ITM15.3	9.0	51.1(5)	7.36(9)	12.8(4)	0.2(1)	0.150(3)	7.66(6)	2.11(8)	14.4(2)	0.75(1)	0.110(6)
ITM16	9.2	48.8(4)	7.48(10)	11.9(4)	0.12(6)	0.050(1)	9.70(7)	1.54(6)	15.8(2)	0.74(1)	n.d.
ITM17	13.6	51.2(5)	8.76(11)	13.8(4)	0.3(1)	0.250(5)	7.76(6)	2.01(8)	12.5(2)	0.98(1)	0.040(2)
ITM19.1	11.0	49.1(4)	7.40(9)	10.9(3)	0.15(7)	0.110(2)	9.21(7)	1.89(8)	16.7(2)	0.80(1)	0.17(1)
ITM19.2	13.6	44.3(4)	7.90(10)	11.7(3)	0.09(4)	0.140(3)	7.84(6)	1.73(7)	20.9(3)	0.85(1)	0.29(2)
ITM20	10.8	47.5(4)	8.17(10)	12.1(4)	0.19(9)	0.080(2)	9.34(7)	1.85(7)	16.0(2)	0.71(1)	0.110(6)
ITM23	8.6	51.6(5)	7.57(10)	12.2(4)	0.2(1)	0.170(4)	8.86(7)	1.23(5)	15.8(2)	1.01(1)	0.150(9)
ITM24	8.0	52.4(5)	7.38(9)	12.1(4)	0.20(9)	0.140(3)	9.18(7)	1.03(4)	15.4(2)	1.00(1)	0.28(2)
IEM26	11.0	48.5(4)	7.94(10)	12.0(4)	0.19(9)	0.130(3)	9.17(7)	1.84(7)	16.5(2)	0.64(1)	0.030(2)
IEM28.1	10.0	47.4(4)	8.74(11)	10.8(3)	0.18(8)	0.130(3)	8.32(6)	1.92(8)	15.9(2)	0.90(1)	0.100(6)
IEM31.2	9.2	52.1(5)	6.08(8)	12.8(4)	0.2(1)	0.220(5)	7.43(6)	2.29(9)	14.4(2)	0.89(1)	0.100(6)
IEM34.1	16.8	50.7(5)	9.84(13)	13.8(4)	0.20(9)	0.230(5)	7.49(6)	1.96(8)	13.2(2)	0.90(1)	0.18(1)
IEM34.3	9.8	47.2(4)	8.46(11)	11.9(4)	0.20(9)	0.110(2)	10.02(8)	1.59(6)	16.3(2)	0.71(1)	0.18(1)
IEM34.4	17.8	50.0(5)	9.98(13)	14.0(4)	0.13(6)	0.170(4)	7.78(6)	1.92(8)	13.0(2)	0.90(1)	0.140(8)
IEM35	9.8	49.5(4)	6.83(9)	10.3(3)	0.16(7)	0.140(3)	8.51(6)	2.30(9)	16.5(2)	0.62(1)	0.110(6)
IEM36	13.2	49.4(4)	7.56(10)	11.9(4)	0.16(7)	0.100(2)	8.45(6)	2.23(9)	16.0(2)	0.66(1)	0.19(1)
IEM37	12.2	52.0(5)	8.47(11)	12.2(4)	0.14(7)	0.170(4)	8.90(7)	1.22(5)	15.2(2)	0.82(1)	0.070(4)
IEM38	15.0	50.2(5)	8.04(10)	13.6(4)	0.18(9)	0.150(3)	8.41(6)	2.26(9)	14.0(2)	1.09(2)	0.140(8)
IEM39	10.4	49.4(4)	7.20(9)	10.3(3)	0.12(6)	0.100(2)	9.16(7)	1.67(7)	16.7(2)	0.92(1)	0.030(2)

Concentrations are given after normalization to 100% on an anhydrous basis. Units in parenthesis represent 1 standard deviation of least units cited; thus, 48.8(4) should be read as 48.8 ± 0.4.

calculate the concentrations of the elements in our samples. For the purpose of this study, only the Ce concentrations are reported in Table 2.

The Pb isotope compositions were measured by multi-collection SIMS 1280 at the NORDSIMS (Stockholm, Sweden). In summary, samples were sputtered with a focused O<sub>2</sub><sup>-</sup> primary beam of 8 nA, with a primary accelerating voltage of 13 kV. After a 90 s pre-sputter with a

25 × 25 μm raster, the raster was stopped during analyses. We used a Kohler illumination method. This resulted in a 15 μm flat-bottomed pit centered in the 25 μm square raster-cleaned area. Secondary positive ions were accelerated at 10 kV and analyzed at mass resolution of 4,800 to resolve all mass interferences. The size of the field aperture was set at 4,000 μm, and the contrast aperture at 400 μm. The centered energy

**Table 2 Volatile elements and cerium concentrations corrected from olivine addition and Pb isotopes in 29 olivine-hosted glassy melt inclusions from Iwate volcano**

	CO <sub>2</sub> ppm	H <sub>2</sub> O wt%	F ppm	S ppm	Cl ppm	Ce ppm	H <sub>2</sub> O/Ce	<sup>207</sup> Pb/ <sup>206</sup> Pb	<sup>208</sup> Pb/ <sup>206</sup> Pb	<sup>206</sup> Pb/ <sup>204</sup> Pb	<sup>207</sup> Pb/ <sup>204</sup> Pb	<sup>208</sup> Pb/ <sup>204</sup> Pb					
ITM1.1	368(140)	2.82(3)	123(2)	1505(20)	408(7)	5.4(2)	5200(700)	0.836	0.002	2.084	0.004	19.20	0.13	16.05	0.12	40.30	0.31
ITM2	315(320)	2.80(1)	164(6)	1071(30)	414(10)	4.7(2)	5900(400)	0.840	0.002	2.081	0.004	18.49	0.10	15.53	0.09	38.75	0.21
ITM5.1	331(5)	2.80(3)	178(1)	1952(10)	394(3)	4.0(1)	7100(300)	0.844	0.004	2.094	0.007	18.31	0.18	15.45	0.13	38.61	0.38
ITM5.2	5(1)	0.77(1)	171(2)	258(2)	350(3)	5.4(3)	1480(90)	0.843	0.001	2.084	0.003	18.56	0.10	15.65	0.08	38.95	0.20
ITM6	28(8)	2.65(1)	155(1)	1527(2)	401(1)	n.d.	n.d.	0.838	0.004	2.084	0.008	18.50	0.30	15.49	0.28	38.80	0.67
ITM8	175(41)	2.74(3)	200(30)	951(14)	423(20)	4.7(4)	5700(1100)	0.840	0.001	2.085	0.004	18.82	0.14	15.81	0.12	39.52	0.30
ITM10.1	479(23)	2.71(1)	159(4)	1273(20)	463(10)	5.1(2)	5300(400)	0.837	0.001	2.081	0.003	18.99	0.12	15.90	0.10	39.81	0.23
ITM11	224(3)	2.57(1)	189(1)	932(5)	387(2)	5.1(2)	5100(200)	0.836	0.002	2.083	0.004	19.23	0.20	16.07	0.16	40.32	0.40
ITM12	6446(200)	2.85(2)	143(1)	1515(8)	405(1)	3.8(1)	7600(300)	0.841	0.002	2.082	0.004	18.86	0.16	15.85	0.13	39.55	0.34
ITM13	3835(590)	2.44(1)	131(3)	1478(40)	372(9)	3.7(2)	6400(600)	0.842	0.003	2.074	0.007	17.74	0.24	14.94	0.19	37.04	0.44
ITM14	32(1)	1.00(1)	138(1)	456(1)	337(2)	4.9(2)	2000(100)	0.839	0.002	2.079	0.003	18.70	0.11	15.68	0.10	39.15	0.23
ITM15.1	n.d.	n.d.	n.d.	n.d.	n.d.	n.d.	n.d.	0.843	0.005	2.091	0.011	19.35	0.21	16.28	0.23	40.70	0.54
ITM15.2	177(110)	2.38(1)	178(1)	644(2)	409(3)	4.1(3)	5900(400)	0.836	0.002	2.084	0.005	18.82	0.12	15.73	0.09	39.49	0.27
ITM16	546(68)	2.28(2)	144(1)	1671(20)	385(3)	4.4(2)	5200(300)	0.841	0.003	2.085	0.007	18.40	0.21	15.46	0.19	38.62	0.40
ITM17	4348(640)	0.62(1)	230(1)	198(1)	427(2)	4.7(2)	1310(90)	0.850	0.002	2.097	0.004	18.43	0.15	15.66	0.11	38.93	0.30
ITM19.1	205(71)	0.41(4)	178(16)	464(40)	406(40)	6.0(3)	690(100)	0.840	0.001	2.084	0.002	18.79	0.07	15.77	0.06	39.44	0.14
ITM23	1071(190)	0.22(1)	196(1)	204(1)	361(2)	5.9(2)	370(30)	0.839	0.001	2.083	0.003	18.84	0.12	15.80	0.10	39.52	0.25
ITM24	77(10)	0.27(1)	204(1)	263(1)	372(2)	6.0(3)	450(40)	0.842	0.001	2.082	0.003	18.63	0.09	15.68	0.07	39.06	0.19
IEM26	755(62)	2.37(3)	173(1)	1805(6)	339(2)	2.9(3)	8200(800)	0.844	0.003	2.089	0.007	18.13	0.18	15.29	0.14	38.13	0.37
IEM28.1	380(6)	3.65(3)	147(1)	1705(10)	352(3)	10(2)	3600(800)	0.843	0.002	2.087	0.004	18.53	0.16	15.61	0.12	38.95	0.32
IEM31.2	4714(440)	0.77(1)	60(1)	287(3)	515(8)	6.9(4)	1120(70)	n.d.	n.d.	n.d.	n.d.	n.d.	n.d.	n.d.	n.d.	n.d.	n.d.
IEM34.1	46(4)	0.82(1)	216(1)	288(1)	393(2)	6.2(2)	1330(70)	0.839	0.001	2.079	0.002	18.63	0.11	15.63	0.09	39.00	0.22
IEM34.3	326(11)	2.44(1)	121(1)	1518(5)	366(2)	2.5(2)	9700(1000)	0.839	0.001	2.091	0.003	19.13	0.11	16.04	0.10	40.27	0.24
IEM34.4	55(4)	0.69(1)	192(1)	951(5)	348(2)	6.4(4)	1070(80)	0.839	0.002	2.089	0.003	18.77	0.08	15.75	0.06	39.47	0.15
IEM35	164(4)	2.94(2)	174(1)	1071(4)	381(3)	4.4(3)	6600(400)	0.837	0.002	2.082	0.004	18.64	0.16	15.60	0.14	39.08	0.34
IEM36	n.d.	n.d.	74(58)	1298(30)	397(30)	3.7(2)	n.d.	n.d.	n.d.	n.d.	n.d.	n.d.	n.d.	n.d.	n.d.	n.d.	n.d.
IEM37	n.d.	n.d.	158(11)	48(25)	448(30)	n.d.	n.d.	0.839	0.001	2.077	0.003	18.34	0.08	15.40	0.07	38.38	0.18
IEM38	n.d.	n.d.	143(96)	407(37)	514(26)	n.d.	n.d.	0.841	0.001	2.076	0.003	18.34	0.10	15.41	0.09	38.34	0.18
IEM39	n.d.	n.d.	n.d.	1058(60)	411(37)	n.d.	n.d.	0.840	0.003	2.069	0.007	18.24	0.20	15.31	0.17	38.01	0.41

Analytical uncertainties are indicated in parenthesis with last significant digits (1 standard deviation of analysis). Errors for Pb-isotope compositions represent 2 standard error of the mean. n.d., not determined. No vapor bubble correction was applied on the volatile concentration measurements in the melt.

window was adjusted to  $\pm 45$  eV. The multicollection system was composed of five ion-counting electron multipliers set on moveable trolleys (L2, L1, C, H1, and H2). The detection array was configured to measure  $^{204}\text{Pb}$  + in the electron multiplier set on the trolley position L2,  $^{206}\text{Pb}$  + in L1,  $^{207}\text{Pb}$  + in C (placed on the ion optical axis) and  $^{208}\text{Pb}$  + in H1. The measurements were conducted over 40 to 120 cycles with a 20 s counting time for each mass and a deadtime correction of 60 ns. A measurement lasted approximately 20 min for 40 cycles. With this setting, the sensitivity on  $^{208}\text{Pb}$  is 19 cts/ppm/nA. Details of Pb measurements are described in Rose-Koga et al. (2012).

## Results

### Major elements

Major element concentrations in melt inclusions are corrected from olivine post-entrapment crystallization and reported in Table 1. They were measured at Laboratoire Magmas et Volcans in Clermont-Ferrand, France, on a Cameca SX 100 using standard procedures outlined in Le Voyer et al. (2008). The Iwate melt inclusions have corrected MgO concentrations between 6.83 and 9.98 wt.% which reach higher values than the range described for the whole rock (3.98 to 7.50 wt.%; Sano et al. 2001). The forsterite values for the olivines range from 70.0 to 80.0 which denotes an evolved magma (Table 3). The melt

inclusions were plotted in a total alkali versus silica (TAS) diagram which classifies them as mainly basaltic with a few exceptions close to the basaltic-andesite domain (Figure 1).

#### Cerium and volatile ( $H_2O$ , $CO_2$ , F, S, Cl) concentrations of melt inclusions

All concentrations are recalculated for olivine post-entrapment crystallization (Table 2). Cerium (Ce) concentrations in Iwate melt inclusions vary between 2.5 and 6.9 ppm with one higher value at 10 ppm. This represents one of the lowest ranges of Ce concentrations among arc melt inclusions. Other arc melt inclusions with low Ce concentration also extend to higher Ce concentrations, for example up to 35 ppm in Lesser Antilles (Bouvier et al. 2010) and up to 30 ppm in Central America (Sadofsky et al. 2008). Iwate thus represents the low end of the range of Ce concentrations in arc melt inclusions.

Iwate melt inclusions have variable concentrations of  $H_2O$ , S, and  $CO_2$  which range from 0.2 to 3.7 wt%  $H_2O$ , 258 to 1,952 ppm S, and 5 to 6,446 ppm  $CO_2$  (Table 2). The volatile contents ( $H_2O$ , S) reach values comparable to other Pacific rim melt inclusions such as Izu Oshima (up to 3.4 wt% and 1,500 ppm, respectively; Ikehata et al. 2009). F concentrations vary between 40 and 230 ppm and Cl concentrations between 337 and 515 ppm (Table 2). The average F and Cl concentration in the melt inclusions is  $156 \pm 44$  ppm and  $399 \pm 45$  ppm, respectively, demonstrating that F and Cl concentrations are relatively low and clustered compared to other Pacific rim melt inclusions (Figure 2). The low F concentrations are similar to those of melt inclusions from oceanic basalts from EPR ( $125 \pm 43$  ppm; Wanless and Shaw 2012), Juan de Fuca ( $117 \pm 12$  ppm; Wanless and Shaw 2012), and Gakkel ridge ( $150 \pm 6$  ppm; Shaw et al. 2010). The Cl concentrations of Iwate melt inclusions are enriched compared to that of melt inclusions from

**Table 3 Major element concentrations (in wt.%) of the 26 Iwate olivines in which glassy melt inclusions where exposed**

Olivine name	Melt incl. name	$SiO_2$	CaO	FeO	MgO	MnO	NiO
ITO1	ITM1.2	39.1 (0.7)	0.14 (0.04)	20.85 (0.73)	40.42 (0.61)	0.38 (0.19)	0.04 (0.021)
ITO2	ITM2	38.2 (0.7)	0.14 (0.05)	23.37 (0.82)	37.93 (0.57)	0.38 (0.19)	0.07 (0.032)
ITO4	ITM5.1; 5.2	38.5 (0.7)	0.17 (0.05)	21.19 (0.74)	39.67 (0.60)	0.30 (0.15)	0.08 (0.039)
ITO5	ITM6	38.5 (0.7)	0.12 (0.04)	21.22 (0.69)	39.40 (0.59)	0.30 (0.15)	0.09 (0.042)
ITO6	ITM8	39.1 (0.7)	0.10 (0.03)	19.73 (0.69)	41.52 (0.62)	0.26 (0.13)	0.06 (0.028)
ITO8	ITM10.1; 10.2	38.9 (0.7)	0.12 (0.04)	20.20 (0.71)	40.66 (0.61)	0.26 (0.13)	0.02 (0.008)
ITO10	ITM11	38.9 (0.7)	0.12 (0.04)	20.92 (0.73)	39.99 (0.60)	0.25 (0.12)	0.05 (0.022)
ITO11	ITM12	39.0 (0.7)	0.14 (0.04)	20.24 (0.71)	40.77 (0.61)	0.29 (0.14)	0.07 (0.031)
ITO12	ITM13	39.1 (0.7)	0.15 (0.05)	19.57 (0.68)	41.30 (0.62)	0.32 (0.16)	0.08 (0.039)
ITO13	ITM14	38.9 (0.7)	0.14 (0.04)	20.33 (0.71)	40.71 (0.61)	0.31 (0.16)	0.07 (0.034)
ITO15	ITM15.1; 15.2	38.5 (0.7)	0.14 (0.05)	23.67 (0.83)	37.78 (0.57)	0.36 (0.18)	0.01 (0.007)
ITO16	ITM16	38.2 (0.7)	0.17 (0.05)	22.08 (0.77)	38.61 (0.58)	0.34 (0.17)	0.05 (0.022)
ITO17	ITM17	38.7 (0.7)	0.16 (0.05)	22.15 (0.78)	38.89 (0.58)	0.38 (0.19)	0.02 (0.007)
ITO19	ITM19.1; 19.2	38.7 (0.7)	0.15 (0.05)	21.22 (0.74)	39.68 (0.60)	0.32 (0.16)	0.07 (0.032)
ITO20	ITM20	38.2 (0.7)	0.15 (0.05)	21.21 (0.74)	39.34 (0.59)	0.36 (0.18)	0.11 (0.052)
ITO24	ITM23	38.4 (0.7)	0.16 (0.05)	22.62 (0.79)	38.63 (0.58)	0.38 (0.19)	0.02 (0.010)
ITO25	ITM24	38.8 (0.7)	0.15 (0.05)	22.77 (0.80)	38.27 (0.57)	0.32 (0.16)	0.03 (0.012)
IEO26	IEM26	38.5 (0.7)	0.15 (0.05)	21.67 (0.76)	39.51 (0.59)	0.32 (0.16)	0.10 (0.046)
IEO28	IEM28.1	39.0 (0.7)	0.12 (0.04)	18.92 (0.66)	42.19 (0.63)	0.29 (0.15)	0.08 (0.037)
IEO31	IEM31.2	37.6 (0.6)	0.15 (0.05)	26.92 (0.94)	35.45 (0.53)	0.40 (0.20)	0.06 (0.028)
IEO34	IEM34.1; 34.3; 34.4	38.7 (0.7)	0.16 (0.05)	20.42 (0.71)	40.29 (0.60)	0.28 (0.14)	0.07 (0.035)
IEO35	IEM35	38.2 (0.7)	0.15 (0.05)	21.47 (0.75)	39.41 (0.59)	0.34 (0.17)	0.05 (0.023)
IEO36	IEM36	38.5 (0.7)	0.15 (0.05)	22.32 (0.78)	39.01 (0.59)	0.32 (0.16)	0.06 (0.027)
IEO37	IEM37	38.7 (0.7)	0.18 (0.06)	20.65 (0.72)	39.98 (0.60)	0.33 (0.17)	0.09 (0.044)
IEO38	IEM38	37.8 (0.6)	0.13 (0.04)	23.30 (0.82)	38.00 (0.57)	0.34 (0.17)	0.05 (0.024)
IEO39	IEM39	39.1 (0.7)	0.12 (0.04)	21.00 (0.74)	40.39 (0.61)	0.38 (0.19)	0.04 (0.021)

Units in parenthesis represent 1 standard deviation.

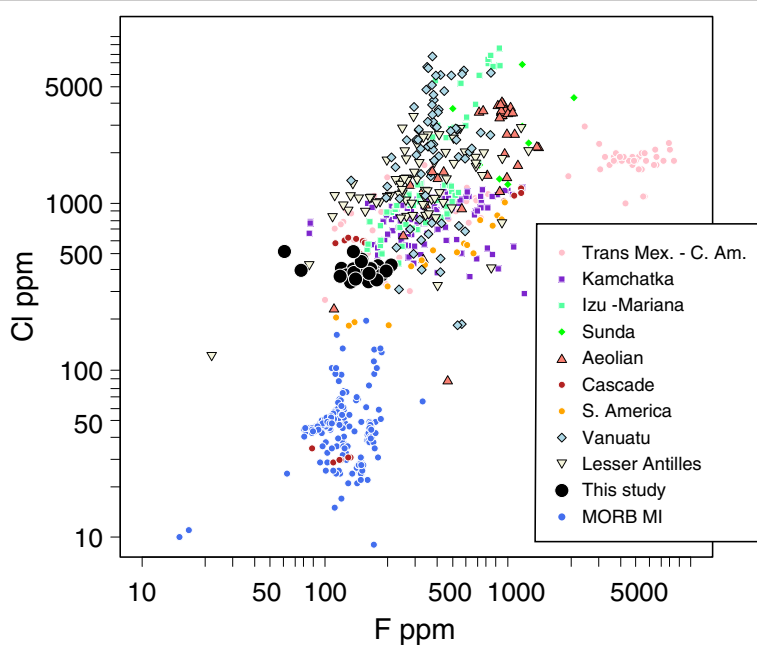


**Figure 2** F concentrations versus Cl concentrations of Iwate melt inclusions (black filled circles). The Iwate melt inclusions are compared to other arc melt inclusions from the literature: Trans Mexican, Vigouroux et al., 2008; Central America, Sadofsky et al., 2008; Kamchatka, Portnyagin et al., 2007; Izu, Straub and Layne, 2003; Sunda, Elburg et al., 2007; Aeolian, Rose-Koga et al., 2012; Le Voyer unpublished data; Cascades, Le Voyer et al., 2010; S. America, Le Voyer et al., 2008; Vanuatu, Sorbadere et al. 2011; and Lesser Antilles, Bouvier et al. 2008, 2010. For MORB melt inclusions, data are from: Gakkel ridge, Shaw et al., 2010; and EPR and Juan de Fuca, Wanless, and Shaw, 2012.

oceanic basalts (EPR,  $44 \pm 10$  ppm; Juan de Fuca,  $61 \pm 32$ ; Gakkel ridge,  $40 \pm 45$  ppm; Wanless and Shaw 2012; Shaw et al. 2010).

#### Pb isotope compositions of melt inclusions

The Pb-isotope compositions of Iwate melt inclusions show more variability than that of their whole rock (Figure 3). This observation is commonly seen among relative abundances of trace elements in melt inclusions because the whole rock often represents an average of separate batches of magma that are trapped in the melt inclusions (e.g., Sobolev and Shimizu 1993; see review by Schiano 2003). The Iwate melt inclusions have Pb isotope compositions  $^{207}\text{Pb}/^{206}\text{Pb}$  between 0.836 to 0.850 and  $^{208}\text{Pb}/^{206}\text{Pb}$  between  $2.069 \pm 0.007$  and  $2.097 \pm 0.004$  (Table 2). These  $^{208}\text{Pb}/^{206}\text{Pb}$  values are equal or higher than that of the neighboring contributing reservoir, the average Pacific oceanic crust (2.055, White et al. 1987), and the average sediments from the Japan Trench (2.067, Plank and Langmuir 1998). The range of  $^{207}\text{Pb}/^{206}\text{Pb}$  variation is within the two endmember values: DMM (0.8570, Hart et al. 1992) and sediments (0.8341, Plank and Langmuir 1998). The melt inclusions' Pb-isotope compositions overlap the literature data of whole rock lower crustal material from NE Japan (Sato 1975; Figure 3).

## Discussion

### Magmatic degassing

$\text{H}_2\text{O}$  concentrations measured in Iwate melt inclusions are at best considered as minimum water concentrations because melt inclusions are leaky containers for  $\text{H}_2\text{O}$  (Chen et al. 2011, 2012; Gaetani et al. 2012). An indication of water loss in Iwate melt inclusions is the weak anti-correlation between  $\text{H}_2\text{O}$  and  $\text{TiO}_2$ . Since availability of  $\text{H}_2\text{O}$  is the principal cause of subarc mantle partial melting,  $\text{H}_2\text{O}$  abundance often correlates with that of other incompatible elements, such as  $\text{TiO}_2$ , among primitive arc magmas (e.g., Kelley et al. 2006; Langmuir et al. 2006). Lack of such anti-correlation suggests the loss of the volatile, incompatible element, hydrogen, from melt inclusions.

The positive correlation between  $\text{H}_2\text{O}$  and S in Iwate melt inclusions then shows degassing of both elements (Figure 4). Sulfur degasses after  $\text{CO}_2$  prior to  $\text{H}_2\text{O}$  saturation, and it exsolves at pressure of about 140 MPa (Spillaert et al. 2006).  $\text{CO}_2$  abundance is less than 1,000 ppm in nearly all the melt inclusions (i.e., five inclusions excluded). These melt inclusions recorded significant pre-entrapment degassing. Therefore, the positive linear correlation (slope 2.32 and correlation coefficient of 0.65) between  $\text{CO}_2$  (for  $\text{CO}_2 < 1,000$  ppm) and S indicates melt degassing prior to entrapment. The

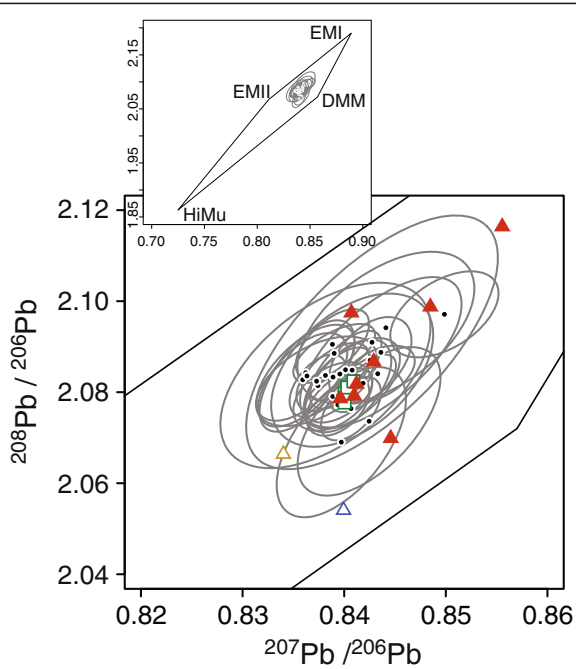


**Figure 3**  $^{208}\text{Pb}/^{206}\text{Pb}$  versus  $^{207}\text{Pb}/^{206}\text{Pb}$  of Iwate glassy melt inclusions.

**Figure 3**  $^{208}\text{Pb}/^{206}\text{Pb}$  versus  $^{207}\text{Pb}/^{206}\text{Pb}$  of Iwate glassy melt inclusions. The compositions are clustered between DMM and EMII mantle endmembers. The ellipses represent the two sigma errors on the measurements. The green squares are the Pb isotope compositions of the Iwate whole rock (Shibata and Nakamura, 1997; Hanyu et al., 2006). The triangles are the local reservoirs (gabbros in filled red, Sato, 1975; Japan Trench sediments in brownish color, Plank and Langmuir, 1998; average Pacific oceanic crust in blue, White et al., 1987). A mixture of these reservoirs can explain the variation in Pb-isotope compositions found in the melt inclusions.

primitive  $\text{CO}_2$ , S, and  $\text{H}_2\text{O}$  concentrations are indeterminable with the current data set. The maximum values we measured are 2,000 ppm for S and  $\approx 4$  wt.% for  $\text{H}_2\text{O}$  which represent the minimum values for primitive S and  $\text{H}_2\text{O}$  contents for Iwate melt inclusions.

F and Cl concentrations in Iwate volcano are clustered (relative standard deviations of F and Cl are 28 and 11%, respectively) and lower than most of other arc melt inclusions (Figure 2). There is no correlation between these halogens and the degassed volatile elements ( $\text{H}_2\text{O}$ ,  $\text{CO}_2$ , and S) which implies that the abundances of F and Cl are likely characterized by processes other than degassing and magma chamber crystallization. The halogens can be used to decipher additional information about the source of the Iwate magma. It should be noted, however, that Cl content is constant over the entire range of  $\text{K}_2\text{O}$  variations (0.07 to 0.25) and  $\text{TiO}_2$  abundance does not correlate with F and Cl.

#### Magma chamber depth and $\text{H}_2\text{O}-\text{CO}_2$ saturation pressure

The degassing of  $\text{CO}_2$  from the magma is obvious when reporting  $\text{H}_2\text{O}$  versus  $\text{CO}_2$  in melt inclusions on a graph along with the saturation curves (SolEx: Witham et al.

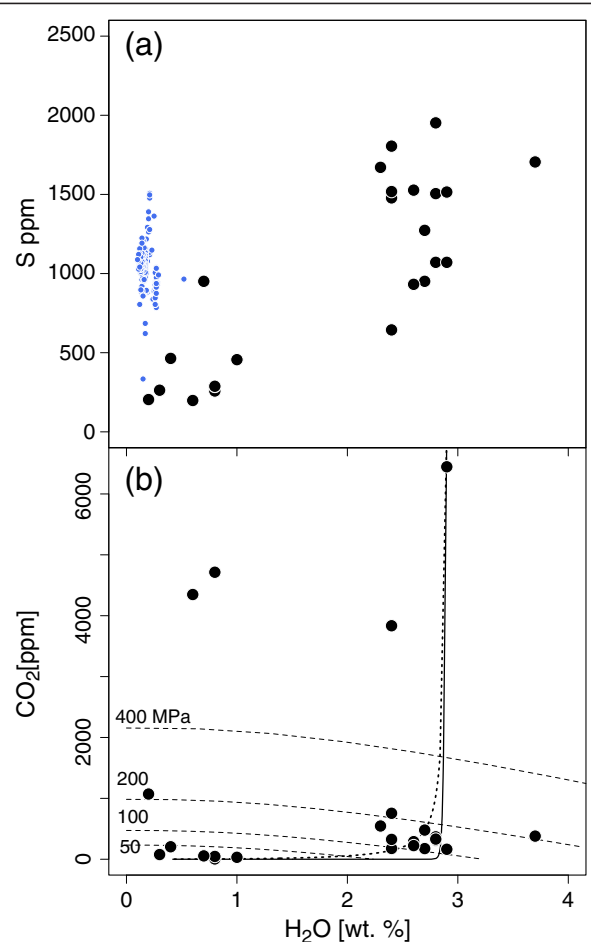


**Figure 4**  $\text{H}_2\text{O}$  versus S and  $\text{H}_2\text{O}$  versus  $\text{CO}_2$  concentrations of

Iwate glassy melt inclusions. (a)  $\text{H}_2\text{O}$  concentrations versus S concentrations of Iwate glassy melt inclusions (black filled circles). The positive correlation is interpreted as a degassing trend of both water and S. For reference, the blue circles are melt inclusions from EPR, Juan de Fuca, and Gakkel ridge basalts (Wanless and Shaw 2012; Shaw et al. 2010). (b)  $\text{H}_2\text{O}$  concentrations versus  $\text{CO}_2$  concentrations of Iwate glassy melt inclusions. The dashed curves are water and  $\text{CO}_2$  saturation curves (Witham et al. 2012); therefore, they define a depth at which the saturation in these molecules is obtained. Since  $\text{H}_2\text{O}$  and  $\text{CO}_2$  concentrations are minimum concentrations (see text for details), the depth of entrapment is imprecise and at best is a minimum estimate. However, we distinguish two groups of inclusions, one with  $\text{H}_2\text{O} < 2$  wt.% and the other with  $\text{H}_2\text{O} > 2$  wt.%. Both groups can be interpreted as representing two degassing trends. Maybe, this reflects the presence of two distinct magma chambers at two different depths as suggested by other geophysical data (see text for details). Solid line indicates an example of open system degassing trajectory; the dotted line indicates closed system degassing.

2012, Figure 4). There are two groups, one with  $\text{H}_2\text{O} < 2$  wt.% and the other with  $\text{H}_2\text{O} > 2$  wt.%. Each trend individually has similar water content and could be classically interpreted as degassing trends in which significant variation of  $\text{CO}_2$  is observed while  $\text{H}_2\text{O}$  remain relatively

constant (Figure 4 degassing trend). During magma ascent, CO<sub>2</sub> degasses first, but this degassing can be sluggish which causes aliquots of melt to be entrapped in the olivine crystals (basalt liquidus forming mineral) prior to complete degassing of CO<sub>2</sub>. This could be the case of the higher CO<sub>2</sub> concentration on both trends. Then H<sub>2</sub>O loss is observed at the end of the trends. The pressure indicated along the curve of Figure 4 cannot be used to estimate precisely the depth of entrapment, because the H<sub>2</sub>O and CO<sub>2</sub> measured concentrations are minimum values. However, the fact that two separate trends coexist could be coincidentally considered as in agreement with the presence of two magma chambers (with slightly different water concentrations) suggested by geophysical data (tomography study and seismic swarms) showing the location of two magma chambers by S-wave velocity slowdowns under Iwate volcano, a crustal magma chamber around 2 km deep and a deeper one around 30 km (Nishida et al. 2008). Long-frequency volcanic swarms are also reported around 30 km depths immediately below the arc crust (Nakajima et al. 2001).

#### Halogen transport

F concentrations of Iwate melt inclusions are in the same range as those reported for MORB melt inclusions (Gakkel from 146 to 166 ppm, Shaw et al. 2010; EPR from 18 to 342 ppm; and Juan de Fuca from 62 to 123 ppm, Wanless and Shaw 2012). Cl concentrations in the Iwate melt inclusions are systematically higher than MORB melt inclusions by approximately an order of magnitude (Figure 2). The enrichment of fluid-mobile elements has been interpreted as a mixing of slab input to the melting region (e.g., Gill 1981; Tatsumi and Eggins 1995). Cl enrichment in arc melt inclusions is observed in multiple studies (Hamada and Fujii 2007; Shaw et al. 2008; Kelley et al. 2010; Rose-Koga et al. 2012; and see review by Wallace 2005). Iwate melt inclusions have a much lower Cl concentration compared to other arc melt inclusions. Other arc volcano melt inclusions rarely plot at lower Cl concentrations than Iwate samples except a few Ecuadorian melt inclusions (Le Voyer et al. 2008), a handful of Mariana melt inclusions (Kelley et al. 2010; Figure 2), and Shasta melt inclusions from dry high-aluminum olivine tholeiite (HAOT; Le Voyer et al. 2010).

Straub and Layne (2003) report significant F and Cl enrichment in clinopyroxene (cpx) and plagioclase-hosted melt inclusions and glass shards from the Izu arc volcanoes. Enrichment of Cl and absence of enrichment of F in Iwate magmas are contrasting characteristics compared to those of Izu and other Cl- and F-rich arc magmas. Simultaneous enrichment of F and Cl in arc lavas is interpreted as the evidence of element addition by aqueous fluid transport from slab to sub-arc mantle (Straub and Layne 2003). However, there is no F

enrichment of Iwate melt inclusions with respect to MORB melt inclusions. Furthermore, Iwate melt inclusions are the Cl- and F-poor endmember of arc melt inclusions. Arc magmas with elevated Cl, with the absence of concomitant F enrichment, therefore enforce the necessity of refining the existing halogen transport model. While the exact cause of the variations seen on the F versus Cl plot is unknown, some magmatic processes are less likely to cause these variations. First, we have argued that degassing of magma before and after entrapment of the inclusion would not be the cause of F and Cl variation. Second, because olivine is the liquidus mineral of basalt in crustal conditions, magma chamber crystal fractionation would not be recorded in primitive olivine melt inclusions. Element fractionation during partial melting and compositional variation of source mantle, perhaps due to metasomatism, are the remaining potential causes of the variation. While element fractionation during partial melting does occur, and F and Cl partition differently in mantle minerals (Dalou et al. 2011 and Table 4), the observed order of magnitude change in F and Cl abundances (between melt inclusions from MORB and Iwate melt inclusions; Figure 3) can only be derived from a highly variable degree of melting of the mantle. Because heterogeneity of non-metasomatized depleted mantle below arcs should have relatively similar composition worldwide (e.g., there are only 40% abundance difference of F between BSE (Lyubetskaya and Korenaga 2007) and DMM (Workman and Hart 2005)), the large F and Cl abundance variations can only be derived from the compositional variation of arc metasomatic agents.

The low F and Cl magma from Iwate contains a significant quantity of H<sub>2</sub>O, consistent with the typical arc magma characteristics. Magma genesis beneath Iwate volcano must be derived from partial melting of a depleted mantle wedge triggered by a water-rich metasomatic agent, typical in arc magmatism. Variation of F and Cl among arc primitive magmas should therefore indicate (1) fractionation processes during transfer of water-rich flux from slab and/or (2) source compositions of the water-rich metasomatic agent.

#### What are the magma sources?

We measured Pb-isotope compositions of the Iwate melt inclusions to decipher the source(s) and/or source mixing in these magmas. The isotopic compositions clusters around a single value (<sup>207</sup>Pb/<sup>206</sup>Pb = 0.840 and <sup>208</sup>Pb/<sup>206</sup>Pb = 2.084), and 81% (22 out of 27) of inclusions are indistinguishable. While the limit of SIMS precision is a partial cause of this homogeneity, the mean Pb composition of Iwate magma is significantly different from depleted mantle (DMM 0.8570 and 2.072; Hart et al. 1992), they actually plot above the tie line between DMM

**Table 4 F and Cl partition coefficients**

D (Mineral/liquid)	F	Cl
(Olivine/basalt)	0.0015 to 0.0047 <sup>a</sup>	<0.0005 <sup>a</sup>
	0.0007 to 0.0033 <sup>b</sup>	
	0.00024 to 0.00054 <sup>e</sup>	
(Clinopyroxene/basalt)	0.039 to 0.067 <sup>a</sup>	<0.01 <sup>a</sup>
	0.043 to 0.153 <sup>c</sup>	0.0017 to 0.021 <sup>c</sup>
	0.086 to 0.153 <sup>d</sup>	0.0086 to 0.0145 <sup>d</sup>
	0.0052 to 0.087 <sup>e</sup>	
(Orthopyroxene/basalt)	0.015 to 0.0448 <sup>a</sup>	0.0017 to 0.028 <sup>c</sup>
	0.031 to 0.037 <sup>b</sup>	
	0.0158 to 0.1233 <sup>c</sup>	
(garnet/basalt)	0.0039 to 0.0174 <sup>a</sup>	<0.007 <sup>a</sup>
	0.0123 <sup>c</sup>	0.0029 <sup>c</sup>
	0.166 <sup>d</sup>	0.087 <sup>d</sup>
(Clinopyroxene/rhyolite)	0.048 to 0.73 <sup>f</sup>	0.065 to 0.158 <sup>f</sup>
(Garnet/rhyolite)	0.028 to 0.12 <sup>f</sup>	0.031 to 0.492 <sup>f</sup>
(Amphibole/basalt)	0.85 to 1.19 <sup>a</sup>	0.038 to 0.046 <sup>a</sup>
	0.36 to 0.63 <sup>d</sup>	0.12 to 0.38 <sup>d</sup>
	0.96 <sup>g</sup>	
(Amphibole/rhyolite)	0.95 to 2.7 <sup>f</sup>	0.079 to 1.87 <sup>f</sup>
(Amphibole/fluid)	7.7 <sup>h</sup>	0.0049 <sup>i</sup>
(Olivine/fluid)	0.11 to 1.4 <sup>j</sup>	0.9 to $2 \times 10^{-4}$ <sup>j</sup>
		0.19 to $1.6 \times 10^{-4}$ <sup>j</sup>
		1.4 to $2 \times 10^{-4}$ <sup>i</sup>
(Clinopyroxene/fluid)		
(Garnet/fluid)	0.014 to 0.26 <sup>i</sup>	0.13 to $13.8 \times 10^{-4}$ <sup>i</sup>
(Orthopyroxene/fluid)	0.0019 to 0.13 <sup>j</sup>	1.5 to $3.7 \times 10^{-4}$ <sup>i</sup>
		0.2 to $6.3 \times 10^{-4}$ <sup>j</sup>

<sup>a</sup>Natural system: Hauri et al. (2006). <sup>b</sup>CMAS and NCMAS system: Beyer et al. (2012). <sup>c</sup>Natural system: Dalou et al. (2011). <sup>d</sup>Natural system: Dalou et al. (manuscript in preparation), Dalou (2011). <sup>e</sup>Natural and Al-free system: O'Leary et al. (2010). <sup>f</sup>Natural system: Van den Bleeken and Koga (submitted to EPSL). <sup>g</sup>Natural system: Adam and Green (2006). <sup>h</sup>Natural system: Wu J, Koga (2013). <sup>i</sup>Natural system: Fabbrizio et al. (2013). <sup>j</sup>MAS system: Bernini et al. (2012).

and EMII (0.81088 and 2.0674; Workman et al. 2004) in a plot of Pb-isotopes normalized to  $^{206}\text{Pb}$  (Figure 3). Mixing of several crustal and oceanic materials containing Pb can explain these compositions, even the range of composition of the basement rocks of NE Japan can alone explain the melt inclusion Pb-isotope compositions (see points on Figure 3). Also, Pb composition of average Pacific oceanic crust and Japan trench sediments loosely bracket the variation (Figure 3). Therefore, isotopic variations recorded in melt inclusions from Iwate volcano show a consistent interpretation. There are three potential sources of Pb identified for Iwate magma: DMM, oceanic crust, and subducted sediments. While Pb isotopes cannot decipher the presence or absence of Pb signature of the basement rock, we argue that melt inclusions hosted in olivine (the first mineral to

crystallize) would unlikely record assimilation process during magma transport through the basement.

The halogens can be used to further constrain the potential sources. F concentration in DMM is 11 ppm (SALTERS and STRACKE 2004), which should produce primitive MORB with F average concentration around  $110 \pm 30$  ppm (an average derived from published melt inclusion data, Figure 2), which is close to the average F in Iwate melt inclusions (i.e., 160 ppm). While F concentrations of other mantle lithologies (EMI, EMII, FOZO, HIMU) are unknown, they are not considered here since variation of Pb isotopes shows none of their presence in the source. As far as F abundance is concerned, any addition of F to the source would produce magmas that are inconsistent with that of Iwate. On the contrary, it is abundantly clear from  $\text{H}_2\text{O}$  and Cl abundances and Pb isotopes that a volatile-rich component was added from the subducted oceanic crust to the magma source.

The abundances of F in different lithologies of subducted oceanic crust should be higher than DMM, while the exact values are yet to be determined. Recent studies of serpentinization at ridges show the increase of F in peridotite sections of oceanic lithosphere up to several 100 s of ppm (Orberger et al. 1999; John et al. 2011; Debret et al. 2013). Fresh MORB contains approximately 100 ppm F, and given that F is insoluble to seawater (1.3 ppm), F content in the basalt section of the oceanic lithosphere must be at least 100 ppm and higher. Sediments are expected to have high F abundance, in the high 100 s (average continent 250 ppm F, pelagic clays 1,300 ppm F, and shale 740 ppm F; Li 1991), while the volume of subducted sediment is probably insignificant compared to that of basalt and peridotite. In any case, it is clear that the metasomatic agent must discriminate F against  $\text{H}_2\text{O}$ , Cl, and Pb.

The presence of significant serpentinite in subducted oceanic lithosphere favors the release of F during prograde metamorphism (Debret et al. 2013). This would lead to increase of F in the subarc mantle. Therefore, we conclude that there is no significant quantity of serpentinites in the subducted lithosphere below Iwate volcano. While present-day seismic tomography imaging may not be directly applicable to magma genesis that took place in the past, no significant quantity of serpentinites is indeed detected below NE Japan (Reynard et al. 2010). The presence of dry slab mantle is also identified by the observation of a strong S-wave velocity jump at the bottom subducted ocean crust detected by receiver function tomography of NE Japan (Kawakatsu and Watada 2007).

The metasomatic agent that is deprived of F must be derived from the basalt and sediment portion of the oceanic lithosphere. F partitions favorably into (dry or wet) silicate melt rather than anyhydrous mantle minerals (olivine, clinopyroxene, orthopyroxene, plagioclase,

Dalou et al. 2011; Table 4). Furthermore, partial melt of hydrous oceanic crust also incorporates more F than anhydrous minerals (garnet, cpx), and shows compatibility for amphibole near unity (Van den Bleeken and Koga, personal communication about submitted manuscript). Therefore, any silicate melt generated in/from the slab would transport similar or higher concentration of F to the magma source region. Therefore, there is no silicate melt below Iwate volcano.

On the contrary, F partition coefficient between hydrous minerals and fluid favors F remaining in the mineral; therefore, aqueous fluid coming from the slab cannot transport significant amounts of F to the sub-arc mantle (Wu and Koga 2013). Because Cl systematically favors fluids over solids (Bernini et al. 2012; Fabbrizio et al. 2013), aqueous fluid is an ideal metasomatic agent that fractionate F from Cl. It should be noted that the salinity of the fluid significantly influences the compatibility of F and Cl. Further refinement of the model is needed to quantify the role of salinity on F/Cl fractionation. The role of supercritical fluid in the source region of Iwate volcano is indeterminable. We speculate that supercritical fluid would favor the transport of high-ionic-strength anions such as F. For Iwate volcano, as it was the case for slab melt, supercritical fluid is unnecessary for the metasomatism of its mantle source.

To summarize, the nature of the slab flux added to the Iwate magma source is an aqueous fluid (in accordance with Hanyu et al. 2006) that must be in equilibrium with hydrous minerals such as amphibole, humite group minerals, and/or mica. This indicates that the temperature at which the aqueous fluid is generated in the slab must not exceed the transition to supercritical fluid or partial melting. For example, it cannot exceed the melting temperature of sediment which is around 700°C for the lowest reported (Nichols et al. 1994). Furthermore, hydrous minerals must be present at the depths of fluid generation, to retain some of the volatile elements (F). For example, amphibole breaks down at pressure above 2.3 to 2.5 GPa (Poli 1993; Van den Bleeken and Koga, submitted) and temperature of 650°C (Poli 1993). On the basis of F concentration variations, we suggest that Iwate volcano represents the low end of the spectrum of slab surface temperatures. This low temperature primarily controls the physical nature of the fluxing agent that originates from the subducted slab and metasomatizes the sub-arc mantle.

#### Low slab surface temperature

Iwate slab surface temperature must be low in order to explain the presence of hydrous phases retaining F in the slab, and aqueous fluid. It must be lower than the melting point of subducted oceanic crust (650 to 700°C after Schmidt and Poli 1998). A recently developed slab

surface thermometer (Plank et al. 2009) is applied to these melt inclusions using H<sub>2</sub>O/Ce ratio. For the melt inclusions with the highest H<sub>2</sub>O concentrations (2.9 wt% in ITM12 and IEM35 and 3.7 wt% in IEM28.1), H<sub>2</sub>O/Ce values predict 720, 740, and 790°C slab surface temperatures, respectively. These predicted temperatures are higher than the solidus. Vice versa, if temperatures lower than the solidus are needed to explain our data (i.e., temperature lower than 650 to 700°C, after Schmidt and Poli 1998), then the measured H<sub>2</sub>O/Ce values of the three most water-rich melt inclusions (7,600, 6,600, and 3,600, respectively) are much lower than the predicted H<sub>2</sub>O/Ce ratio of aqueous fluid (10<sup>5</sup> to 10<sup>6</sup>, Plank et al. 2009). Therefore, we conclude that metasomatism of subarc mantle by aqueous fluid, is in discord with melt forming temperature inferred from H<sub>2</sub>O/Ce.

It should be noted that the loss of H<sub>2</sub>O through degassing can drive the H<sub>2</sub>O/Ce to lower values. Similarly, crystal fractionation can increase Ce concentration. While these Iwate melt inclusions hosted in olivine are glassy and sampled from scoria, they may have somehow failed to retain the H<sub>2</sub>O and Ce source character predicted by the thermometer of Plank et al. (2009). Geochemical indicators involving highly volatile elements, such as H<sub>2</sub>O/Ce, may in fact be applicable to a limited number of samples that can meet stringent criteria proving non-degassing. Furthermore, the thermometer calibration is potentially limited to a narrow range of slab compositions at a 4-GPa condition. Indiscriminate application of the slab surface thermometer to arc melt inclusions would lead to an erroneous temperatures.

#### Competing interests

The authors declare that they have no competing interests.

#### Authors' contribution

ERK prepared the samples, participated to the measurements, and drafted the manuscript. KTK participated to the isotope measurements and drafted the manuscript. MH provided the scoria samples and initiated ERK's interest in Iwate and edited the manuscript. TH performed most of the electron probe measurements during his short internship as a 'L3-student' in the lab. NS and MW helped a great deal in fine-tuning the SIMS to appease our wish of precision and participated to the edition of the manuscript. All authors read and approved the final manuscript.

#### Acknowledgements

ERK thanks JL Devidal for his precious guidance during the electron probe analysis. ERK is indebted to Cedrick O'Shaughnessy for the final proof reading of the manuscript. The authors acknowledge financial support from the French Agence Nationale de la Recherche (projects: SlabFlux grant no. ANR 2009 Blanc 0338 and DegazMag, grant no. ANR 2011 Blanc SIMI 5-6 003). This research was financed by the French Government Laboratory of Excellence initiative no. ANR-10-LABX-0006, the Région Auvergne, and the European Regional Development Fund. This is Laboratory of Excellence ClerVolc contribution no. 107. The NordSIMS facility is financed and operated under a joint Nordic contract; this is NordSIMS contribution no. 377.

#### Author details

<sup>1</sup>Laboratoire Magmas et Volcans, Université Blaise Pascal, CNRS, UMR 6524, IRD, R 163, Clermont-Ferrand 63038, France. <sup>2</sup>Department of Solid Earth

Geochemistry, Institute for Research on Earth Evolution (IFREE), Japan Agency for Marine-Earth Science and Technology (JAMSTEC), 2-15 Natsushima-cho, Yokosuka 237-0061, Japan. <sup>3</sup>Laboratory for Isotope Geology, Swedish Museum of Natural History, Stockholm, SE-104 05, Sweden. <sup>4</sup>Woods Hole Oceanographic Institution, Woods Hole, MA 02543, USA.

Received: 25 November 2013 Accepted: 11 July 2014

Published: 1 August 2014

## References

- Adam J, Green TH (2006) Trace element partitioning between mica- and amphibole-bearing garnet Iherzolite and hydrous basanitic melt: 1. Experimental results and the investigation of controls on partitioning behaviour. *Contrib Mineral Petrol* 152:1–17
- Bernini D, Wiedenbeck M, Dolejš D, Keppler H (2012) Partitioning of halogens between mantle minerals and aqueous fluids: implications for the fluid flow regime in subduction zones. *Contrib Mineral Petrol* 165:117–128
- Beyer C, Klemme S, Wiedenbeck M, Stracke A, Vollmer C (2012) Fluorine in nominally fluorine-free mantle minerals: experimental partitioning of F between olivine, orthopyroxene and silicate melts with implications for magmatic processes. *Earth Planet Sci Lett* 337–338:1–9
- Bouvier AS, Métrich N, Deloule E (2008) Slab-derived fluids in the magma sources of St. Vincent (Lesser Antilles Arc): volatile and light element imprints. *J Petrol* 49:1427–1448, doi:10.1093/petrology/egn031
- Bouvier AS, Deloule E, Métrich N (2010) Fluid Inputs to Magma Sources of St. Vincent and Grenada (Lesser Antilles): New Insights from Trace Elements in Olivine-hosted Melt Inclusions. *J Petrol* 51:1597–1615
- Chen Y, Provost A, Schiano P, Cluzel N (2011) The rate of water loss from olivine-hosted melt inclusions. *Contrib Mineral Petrol* 162:625–636, doi:10.1007/s00410-011-0616-5
- Chen Y, Provost A, Schiano P, Cluzel N (2012) Magma ascent rate and initial water concentration inferred from diffusive water loss from olivine-hosted melt inclusions. *Contrib Mineral Petrol* 165:525–541, doi:10.1007/s00410-012-082-x
- Dalou C, Koga KT, Shimizu N, Boulon J, Devidal JL (2011) Experimental determination of F and Cl partitioning between Iherzolite and basaltic melt. *Contrib Mineral Petrol* 163:591–609
- Dalou C, Koga KT, Le Voyer M, Shimizu N (2013) Experimental determination of f and cl partition coefficients between anhydrous minerals and hydrous basaltic melts: implications of cl/f signature in arc magmas, manuscript in preparation
- Dalou C (2011) Fluorine and Chlorine fractionation in the sub-arc mantle: an experimental investigation, thesis. Université Blaise Pascal Clermont-Ferrand, France
- Debret B, Koga KT, Niccollet C, Andreani M, Schwartz S (2013) F, Cl and S input via serpentinite in subduction zones: implications for the nature of the fluid released at depth. *Terra Nova* 26:96–101, doi:10.1111/ter.12074
- Elburg MA, Kamenetsky VS, Foden JD, Sobolev A (2007) The origin of medium-K ankaramitic arc magmas from Lombok (Sunda arc, Indonesia): Mineral and melt inclusion evidence. *Chem Geol* 240:260–279, doi:10.1016/j.chemgeo.2007.02.015
- Fabbrizio A, Stalder R, Hametner K (2013) Experimental chlorine partitioning between forsterite, enstatite and aqueous fluid at upper mantle conditions. *Geochim Cosmochim Acta* 121:684–700
- Gaetani GA, O'Leary JA, Shimizu N, Bucholz CE, Newville M (2012) Rapid reequilibration of H<sub>2</sub>O and oxygen fugacity in olivine-hosted melt inclusions. *Geology* 40:915–918, doi:10.1130/G32992.1
- Gill JB (1981) Orogenic Andesites and Plate Tectonics, 390 p. Springer, New York, doi:10.1007/978-3-642-68012-0
- Hamada M, Fujii T (2007) H<sub>2</sub>O-rich island arc low-K tholeiite magma inferred from Ca-rich plagioclase-melt inclusion equilibria. *Geochemical Journal* 41:437–461
- Hanyu T, Tatsumi Y, Nakai S, Chang Q, Miyazaki T, Sato K, Tani K, Shibata T, Yoshida T (2006) Contribution of slab melting and slab dehydration to magmatism in the NE Japan arc for the last 25 Myr: constraints from geochemistry. *Geochem Geophys Geosyst* 7, doi:10.1029/2005GC001220
- Hart SR, Hauri EH, Oschmann L, Whitehead J (1992) Mantle plumes and entrainment: isotopic evidence. *Science* 256:517–520
- Hauri EH, Gaetani GA, Green TH (2006) Partitioning of water during melting of the Earth's upper mantle at H<sub>2</sub>O-undersaturated conditions. *Earth Planet Sci Lett* 248:715–734
- Heiro C, Longpré M-A, Shimizu N, Clague DA, Stix J (2011) Explosive eruptions at mid-ocean ridges driven by CO<sub>2</sub>-rich magmas. *Nat Geosci* 4:260–263, doi:10.1038/ngeo1104
- Ikehata K, Yasuda A, Notsu K (2009) The geochemistry of volatile species in melt inclusions and sulfide minerals from Izu-Oshima volcano, Japan. *Miner, Petrol* 99:143–152, doi:10.1007/s00710-009-0086-x
- Itoh J, Doi N (2005) Geological map of Iwate volcano. Geological Survey of Japan, National Institute of Advanced Industrial Science and Technology (in Japanese with English abstract)
- John T, Scambelluri M, Frische M, Barnes JD (2011) Dehydration of subducting serpentinite: Implications for halogen mobility in subduction zones and the deep halogen cycle. *Earth Planet Sci Lett* 308:65–76
- Kawakatsu H, Watada S (2007) Seismic evidence for deep-water transportation in the mantle. *Science* 316:1468–1471, doi:10.1126/science.1140855
- Kelley KA, Plank T, Grove TL, Stolper EM, Newman S, Hauri EH (2006) Mantle melting as a function of water content beneath back-arc basins. *J Geophys Res* 111, doi:10.1029/2005JB003732
- Kelley KA, Plank T, Newman S, Stolper EM, Grove TL, Parman S, Hauri EH (2010) Mantle Melting as a Function of Water Content beneath the Mariana Arc. *Journal of Petrology* 51:1711–1738, doi:10.1093/petrology/egg036
- Kuritani T, Yoshida T, Kimura J-I, Hirahara Y, Takahashi T (2013) Water content of primitive low-K tholeiitic basalt magma from Iwate Volcano, NE Japan arc: implications for differentiation mechanism of frontal-arc basalt magmas. *Contrib. Miner Petrol* 108:1–11, doi:10.1007/s00710-013-0278-2
- Langmuir CH, Bezoz A, Escrig S, Parman SW (2006) Chemical systematics and hydrous melting of the mantle in back-arc basins. *American Geophysical Union Monograph Series*, Washington, D. C., pp 87–146
- Le Voyer M, Rose-Koga EF, Laubier M, Schiano P (2008) Petrogenesis of arc lavas from the Rucu Pichincha and Pan de Azucar volcanoes (Ecuadorian arc): major, trace element, and boron isotope evidences from olivine-hosted melt inclusions. *Geochem Geophys Geosyst* 9, doi:10.1029/2008GC002173
- Le Voyer M, Rose-Koga EF, Shimizu N, Grove TL, Schiano P (2010) Two contrasting H<sub>2</sub>O-rich components in primary melt inclusions from Mount Shasta. *J Petrol* 51:1571–1595, doi: 10.1093/petrology/egg030
- Li Y (1991) Distribution patterns of the elements in the ocean: a synthesis. *Geochim Cosmochim Acta* 55:3223–3240
- Lyubetskaya T, Korenaga J (2007) Chemical composition of Earth's primitive mantle and its variance: 1. Method and results. *Journal of Geophysical Research: Solid Earth* 112:B30211, doi:10.1029/2005JB004223
- Nakajima J, Matsuzawa T, Hasegawa A, Zhao D (2001) Seismic imaging of arc magma and fluids under the central part of northeastern Japan. *Tectonophysics* 340:1–17
- Nakamura H, Iwamori H (2009) Contribution of slab-fluid in arc magmas beneath the Japan arcs. *Gondwana Research* 16:431–445, doi: 10.1016/j.gr.2009.05.004
- Nichols GT, Wyllie PJ, Stern CR (1994) Subduction zone melting of pelagic sediments constrained by melting experiments. *Nature* 371:785–788, doi:10.1038/371785a0
- Nishida K, Kawakatsu H, Obara K (2008) Three-dimensional crustal S-wave velocity structure in Japan using microseismic data recorded by Hi-net tiltmeters. *J Geophys Res* 113, doi:10.1029/2007JB005395
- O'Leary J, Gaetani GA, Hauri EH (2010) The effect of tetrahedral Al<sup>3+</sup> on the partitioning of water between clinopyroxene and silicate melt. *Earth Planet Sci Lett* 297:111–120
- Orberger B, Métrich N, Mosbah M, Mével C (1999) Nuclear microprobe analysis of serpentine from the mid-Atlantic ridge. *Nuclear Instruments and Methods in Physics Research B* 158:575–581
- Plank T, Langmuir CH (1998) The chemical composition of subducting sediment and its consequences for the crust and mantle. *Chem Geol* 145:1–70
- Plank T, Cooper LB, Manning CE (2009) Emerging geothermometers for estimating slab surface temperatures. *Nature Geoscience* 2:611–615, doi:10.1038/ngeo614
- Poli S (1993) The amphibolite-eclogite transformation; an experimental study on basalt. *Am J Sci* 293:1061–1107
- Portnyagin M, Hoernle K, Plechov P, Mironov N (2007) Constraints on mantle melting and composition and nature of slab components in volcanic arcs from volatiles (H<sub>2</sub>O, S, Cl, F) and trace elements in melt inclusions from the Kamchatka Arc. *Earth Planet Sci Lett* 255:53–69
- Reynard B, Nakajima J, Kawakatsu H (2010) Earthquakes and plastic deformation of anhydrous slab mantle in double Wadati-Benioff zones. *Geophys Res Lett* 37, doi:10.1029/2010GL045494

- Rose-Koga EF, Shimizu N, Devidal JL, Koga KT, Le Voyer M, Dobeli M (2008) Investigation of F, S and Cl standards by ion probe and electron microprobe. AGU conference abstract, Fall
- Rose-Koga EF, Koga K, Schiano P, Le Voyer M (2012) Mantle source heterogeneity for South Tyrrhenian magmas revealed by Pb isotopes and halogen contents of olivine-hosted melt inclusions. *Chem Geol* 334:266–279
- Sadowsky SJ, Portnyagin M, Hoernle K (2008) Subduction cycling of volatiles and trace elements through the Central American volcanic arc: evidence from melt inclusions. *Contrib. Mineral Petro* 155:433–456, doi:10.1007/s00410-007-0251-3
- Salter JWM, Stracke A (2004) Composition of the depleted mantle. *Geochem Geophys Geosyst* 5, doi:10.1029/2003GC000597
- Sano T, Hasenaka T, Shimaoka A, Yonezawa C, Fukuoka T (2001) Boron contents of Japan Trench sediments and Iwate basaltic lavas, Northeast Japan arc: estimation of sediment-derived fluid contribution in mantle wedge. *Earth Planet Sci Lett* 186:187–198
- Sato K (1975) Unilateral isotopic variation of Miocene ore leads from Japan. *Econ Geol* 70:800–805
- Schiano P (2003) Primitive mantle magmas recorded as silicate melt inclusions in igneous minerals. *Earth-Science Reviews* 63:121–144, doi:10.1016/S0012-8252(03)00034-5
- Schmidt MW, Poli S (1998) Experimentally based water budgets for dehydrating slabs and consequences for arc magma generation. *Earth Planet Sci Lett* 163:361–379
- Shaw AM, Hauri EH, Fischer TP, Hilton DR, Kelley KA (2008) Hydrogen isotopes in Mariana arc melt inclusions: implications for subduction dehydration and the deep-Earth water cycle. *Earth Planet Sci Lett* 275:138–145, doi:10.1016/j.epsl.2008.08.015
- Shaw AM, Behn MD, Humphris SE, Sohn RA, Gregg PM (2010) Deep pooling of low degree melts and volatile fluxes at the 85°E segment of the Gakkel Ridge: evidence from olivine-hosted melt inclusions and glasses. *Earth Planet Sci Lett* 289:311–322, doi:10.1016/j.epsl.2009.11.018
- Shibata T, Nakamura E (1997) Across-arc variations of isotope and trace element compositions from Quaternary basaltic volcanic rocks in northeastern Japan: Implications for interaction between subducted oceanic slab and mantle wedge. *J Geophys Res* 102:8051–8064
- Shimizu N, Hart SR (1982) Applications of the ion microprobe to geochemistry and cosmochemistry. *Ann Rev Earth Planet Sci* 10:483
- Shishkina TA, Botcharnikov RE, Holtz F, Almeev RR, Portnyagin MV (2010) Solubility of H<sub>2</sub>O- and CO<sub>2</sub>-bearing fluids in tholeiitic basalts at pressures up to 500 MPa. *Chem Geol* 277:115–125, doi:10.1016/j.chemgeo.2010.07.014
- Sobolev A, Shimizu N (1993) Ultra-depleted primary melt included in an olivine from the Mid-Atlantic Ridge. *Nature* 363:151
- Sobolev AV (1996) Melt inclusions in minerals as a source of principle petrological information. *Petrology* 4:209–220
- Sorbadere F, Schiano P, Métrich N, Garaebiti E (2011) Insights into the origin of primitive silica-undersaturated arc magmas of Aoba volcano (Vanuatu arc). *Contributions to Mineralogy and Petrology* 162:995–1009, doi:10.1007/s00410-011-0636-1
- Spilliaert N, Métrich N, Allard P (2006) S-Cl-F degassing pattern of water-rich alkali basalt: modelling and relationship with eruption styles on Mount Etna volcano. *Earth Planet Sci Lett* 248:772–786, doi:10.1016/j.epsl.2006.06.031
- Straub SM, Layne GD (2003) The systematics of chlorine, fluorine, and water in Izu arc front volcanic rocks: implications for volatile recycling in subduction zones. *Geochim Cosmochim Acta* 67:4179–4203, doi:10.1016/S0016-7037(03)00307-7
- Tatsumi Y, Eggin S (1995) Subduction zone magmatism, 211 p. Blackwell Sci, Cambridge, U. K
- Van den Bleeken G, Koga KT Experimentally determined distribution of fluorine and chlorine upon hydrous melting of subducted oceanic crust and calculated fluxes, submitted
- Vigouroux N, Wallace PJ, Kent AJR (2008) Volatiles in high-K magmas from the Western Trans-Mexican Volcanic Belt: evidence for fluid fluxing and extreme enrichment of the mantle wedge by subduction processes. *J Petrol* 49:1589–1618, doi:10.1093/petrology/egn039
- Wallace PJ (2005) Volatiles in subduction zone magmas: concentrations and fluxes based on melt inclusion and volcanic gas data. *J Volcanol Geotherm Res* 140:217–240, doi:10.1016/j.jvolgeores.2004.07.023
- Wanless VD, Shaw AM (2012) Lower crustal crystallization and melt evolution at mid-ocean ridges. *Nat Geosci* 5:651–655, doi:10.1038/ngeo1552
- White WM, Hofmann AW, Puchelt H (1987) Isotope geochemistry of Pacific Mid-Ocean Ridge Basalt. *Journal of Geophysical Research* 92:4881, doi:10.1029/JB092iB06p04881
- Witham F, Blundy J, Kohn SC, Lesne P, Dixon JE, Churakov SV, Botcharnikov R (2012) Computers & Geosciences. *Comput Geosci* 45:87–97
- Workman RK, Hart SR, Jackson MG, Regelous M, Farley KA, Bluszczajn J, Kurz MD, Staudigel H (2004) Recycled metasomatized lithosphere as the origin of the Enriched Mantle II (EM2) end-member: Evidence from the Samoan Volcanic Chain. *Geochem Geophys Geosys* 5:44
- Workman RK, Hart SR (2005) Major and trace element composition of the depleted MORB mantle (DMM). *Earth and Planetary Science Letters* 231:53–72, doi:10.1016/j.epsl.2004.12.005
- Wu J, Koga KT (2013) Fluorine partitioning between hydrous minerals and aqueous fluid at 1 GPa and 770–947 °C: a new constraint on slab flux. *Geochim Cosmochim Acta* 119:77–92
- Wyss M, Hasegawa A, Nakajima J (2001) Source and path of magma for volcanoes in the subduction zone of northeastern Japan. *Geophys Res Lett* 28:1819–1822

doi:10.1186/1880-5981-66-81

**Cite this article as:** Rose-Koga et al.: Volatile (F and Cl) concentrations in Iwate olivine-hosted melt inclusions indicating low-temperature subduction. *Earth, Planets and Space* 2014 **66**:81.

**Submit your manuscript to a SpringerOpen® journal and benefit from:**

- Convenient online submission
- Rigorous peer review
- Immediate publication on acceptance
- Open access: articles freely available online
- High visibility within the field
- Retaining the copyright to your article

Submit your next manuscript at ► [springeropen.com](http://springeropen.com)